Study on the spectrum characteristics of rock burst and the stability of the surrounding rock of a roadway in mines under dynamic load

Yang yushun (cqyysh@126.com)
Chongqing University https://orcid.org/0000-0002-8510-7194
Sijiang Wei
Henan Polytechnic University
Kui Li
Henan Polytechnic University

Research

Keywords: rock burst, frequency spectrum characteristics, dynamic load, numerical simulation, mechanism analysis

Posted Date: August 10th, 2021

DOI: https://doi.org/10.21203/rs.3.rs-746641/v1

Study on the spectrum characteristics of rock burst and the stability of the surrounding rock of a roadway in mines under dynamic load

Yushun Yang [a*], Sijiang Wei [b,c], Kui Li [b]

[a] Faculty of Architecture and Civil Engineering, Huaiyin Institute of Technology, Huai'an 223001, China;

[b] School of Energy Science and Engineering, Henan Polytechnic University, Jiaozuo 454003, China;

[c] The Collaborative Innovation Center of Coal Safety Production in Henan Province, Jiaozuo 454003, China.

* Correspondence: cqyysh@126.com

Abstract: This study analyzes the impact pressure in the Yuejin and Qianqiu coal mines in the Yimei mine area, and shows that rock bursts may be caused by damage to the overburden gravel strata caused by coal seam mining and unreasonable mining layout. Rock burst microseismic signals from the Yuejin and Qianqiu mines show that the duration of the vibration waveform is greater than 0.06 s. The fast Fourier transform shows that the low-frequency component of the rock burst accounts for a large proportion, with the main frequency being concentrated in the range between 5 and 50 Hz. A numerical simulation scheme was designed, and the extended D-P strength criterion was adopted to select the distributed load of a sinusoidal pulse in the load waveform as the dynamic load. The plastic strain energy density distribution is used to measure the tendency of the surrounding rock to impact the roadway. By changing the shock position, wave frequency, disturbance intensity, tunnel section shape, and buried depth, it is seen that when a (vibration wave amplitude) = 2.0 m/s^2, f (vibration wave frequency) = 40 Hz, H (roadway buried depth) = 1000 m, θ (the angle between the impact position of the seismic wave and the center of the roadway) = 180°, and the roadway section is horseshoe-shaped, the tendency of the surrounding rock to impact the roadway is higher. Under the same conditions, the impact tendency of the surrounding rock on the roadway is the smallest and second smallest when the roadway is circular and straight-wall arched, respectively.

Keywords: rock burst; frequency spectrum characteristics; dynamic load; numerical simulation; mechanism analysis

Introduction

With the continuous increase in the mining depth and intensity of exploring and exploiting coal resources, dynamic disasters, such as rock bursts, during the process of mining coal resources have become increasingly exacerbated. By 2020, there were 133 rock bursts in mines in China [1], of which 50 mines with a mining depth of more than 1000 m had rock bursts. Rock bursts lead to serious roadway deformation,

support breakage, rib spalling and roof fall, and casualties, which seriously threaten the safe and efficient mining of coal resources [2-4].

For a long time, scholars at home and abroad have paid attention to the mechanism and prevention of coal mine rock burst. Qian [5] divided rockburst into fault slip or shear fracture induced rockburst and strain type rockburst induced by rock failure according to different mechanism of rockburst. Combined with accident cases, the occurrence mechanism and characteristics of strain type and slip type rockburst and rock burst were analyzed. Pan et al. [6] established the dynamic response differential equation of surrounding rock and support under rock burst, and proposed the control method of surrounding rock of roadway under rock burst. Dou et al. [7] carried out the research on the identification of acoustic and seismic precursors in the process of coal and rock disaster by means of laboratory acoustic emission and stope microseismic monitoring, and proposed a comprehensive early warning model of rock burst based on microseismic precursor index system. Yang and Wei [8] used CDEM software to simulate and study the mechanical properties of surrounding rock of deep roadway under the conditions of uniaxial compressive strength, disturbance stress, frequency, buried depth and wave propagation angle. Jin et al. [9] conducted three-dimensional dynamic compression tests on red sandstone under different static stress and impact velocity. Xia et al. [10] established the static comprehensive evaluation index and method of impact risk, aiming at the problems of critical mutation and difficulty in weight quantification in impact risk evaluation by comprehensive index method and multi factor coupling method. Song et al. [11] analyzed the stress distribution characteristics and microseismic activity law of surrounding rock in coal seam gangue occurrence area under dynamic and static load conditions, which provided a reference for the prevention and control of rock burst in coal face with gangue. Jiao [12] quantitatively studied the influence law of single factor such as surrounding rock strength, source distance, source strength, original rock stress, support strength and multi factor interaction on the deformation of roadway anchorage bearing structure. Wang et al. [13] used UDEC numerical simulation to study the stress distribution and evolution in different pushing and mining directions of adjacent fault working face under hard and thick roof, and analyzed the influence and difference of pushing and mining direction on stress characteristics and induced impact potential risk main control area. He et al. [14] carried out the experimental research on mechanical response of commonly used pallets and their combined components in coal mines by using the drop weight impact test device, revealed the impact resistance mechanical performance of bolting surface components, and provided design basis for the selection of bolting surface components in rock burst roadway. Based on the particularity of graben

structure and the occurrence characteristics of overburden. Wu et al. [15] analyzed the movement characteristics of overburden and the stress evolution law of coal and rock mass in the graben structure area, established the corresponding mechanical model, and studied the mechanism of rock burst in the graben structure area. Cui et al. [16] analyzed the mining disturbance characteristics under different advancing speed and mining thickness, and discussed the application of mining disturbance characteristics in mine productivity control and mining method optimization.

To summarize, during rock excavation, dynamic mine disasters caused by the sudden release of high stress from the surrounding rock and dynamic disturbance load have complex dynamic characteristics. Therefore, this study analyzes the causes of rock bursts and the frequency spectrum characteristics of vibration waveforms of these rock bursts in the Yuejin and Qianqiu mines in the Yi coal mine area. A numerical simulation scheme is designed to simulate the response characteristics of different influencing factors on the surrounding rock of roadways under dynamic load to provide theoretical guidance to control the impact of surrounding rock under dynamic load on roadways.

Spectrum characteristics of rock bursts

Frequent microearthquakes have occurred in the Yuejin and Qianqiu mines, causing difficulties for safe and efficient mining. To predict the precursor information of rock bursts, an ESG microseismic monitoring system has been installed in the mine. In this study, the seismic waveform collected during the occurrence of rock bursts was analyzed, and a fast Fourier transform was carried out using MATLAB software to analyze the spectrum characteristics of the rock bursts to guide subsequent research.

Spectrum characteristics of the Yuejin Mine

There have been many rock burst accidents in the Yuejin coal mine during the mining of the working face. From July 17, 2010, to September 16, 2010, three rock burst incidents with obvious destruction occurred in the lower roadway of the 25110 working face, with a source level of 2.7 and energy of 9×107 J. Many workers were injured. The 480 m–842.8 m section of the lower roadway of the working face was impacted, and the roadway was seriously damaged. The 430 m–480 m section of the belt rack overturned downward, the floor heaved slightly, and the upper roadway 120 m from the upper turning head was slightly damaged. Since the probe used in the microseismic monitoring system is a velocity sensor, the vibration signal is a velocity time history curve. Fig. 1 and Fig. 2 show the velocity time vibration signal and corresponding

spectrum characteristics of the three rock bursts respectively.

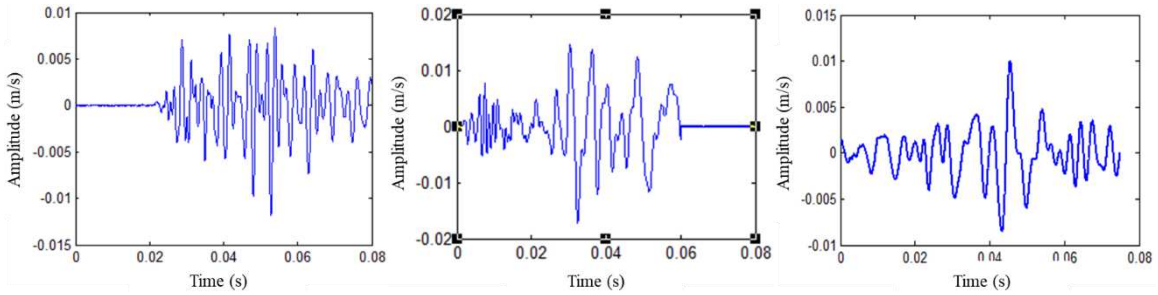

(a) first (b) second (c) third

Fig. 1. Waveforms of the three rock bursts in the Yuejin Mine

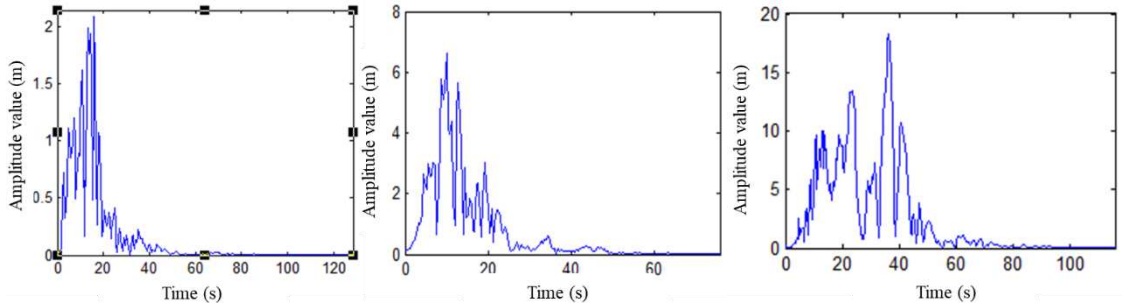

(a) first (b) second (c) third

Fig. 2. Waveform of the three rock bursts in the Yuejin Mine

It can be seen from Fig. 1 – 2 that the amplitude range of the main shock wave of the vibration waveform is -0.02–0.02 m/s. Low-frequency components, concentrated in the range of 0–60 Hz, account for a large proportion. The main frequency of the first shock event is concentrated in the range of 0–40 Hz, and the maximum amplitude is 18 Hz, of which 0–20 Hz accounts for 51.2%, 20–40 Hz for 38.4%, and 40–60 Hz for 10.4%. The main frequency of the second shock event is concentrated in the range 0–40 Hz, and the maximum amplitude is 10 Hz, of which 0–20 Hz accounts for 62.5%, 20–40 Hz for 28.4%, and 40–60 Hz for 9.4%. The main frequency of the third shock event is concentrated in the range of 0–40 Hz, and the maximum amplitude is 38 Hz, of which 0–40 Hz accounts for 58.4%, 40–60 Hz accounts for 30.4%, and greater than 60 Hz accounts for 12.2%.

Spectrum characteristics of the Qianqiu mine

In February 2014, three rock burst events occurred in the 21032 return wind uphill of the Qianqiu mine, with an energy of 1.1% × 10^7J and a magnitude of 1.9. The impact event occurred in the roof. When the rock burst occurred, the roadway 85 m above the return air connecting roadway and 20 m away from the lower slope changing point was damaged to varying degrees. The roadway 50 m away from the lower slope changing point was seriously damaged, and the roadway was basically closed. There was only about 0.8 m of space on the lower side of the roadway. Most of the 36 u embracing pillars in the roadway were bent, and

the two air doors in the lower parking lot were damaged by the shock wave; the gas concentration was as high as 9%, and the 763 belt inclined roadway, the strong belt head chamber, and the three-meter winch room in mining area 21 were deformed to varying degrees. Fig. 2 shows the velocity time vibration signal diagram and the corresponding spectrum characteristic of the three rock bursts.

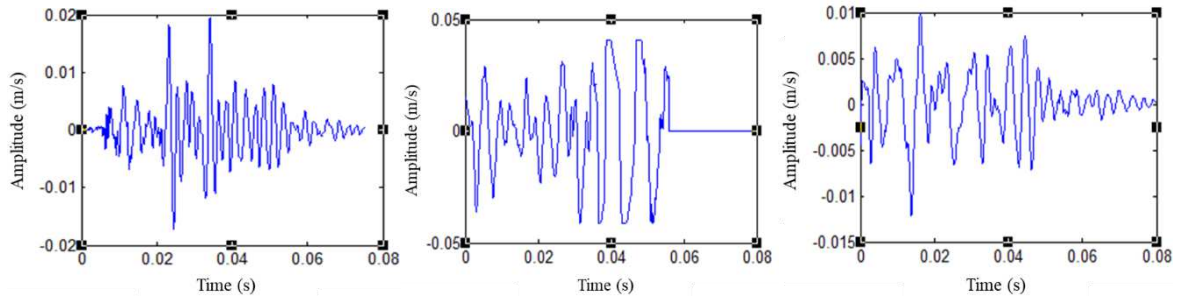

(a) first (b) second (c) third

Fig. 3. Waveform of the three rock bursts in the Qianqiu mine

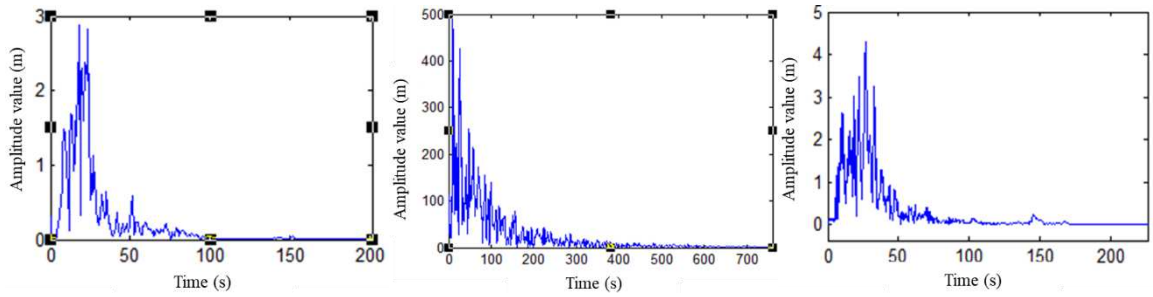

(a) first (b) second (c) third

Fig. 4. Waveform of the three rock bursts in the Qianqiu mine

It can be seen from Fig. 3 – 4 that the amplitude of the main shock wave of the vibration waveform ranges from -0.015 to 0.05m/s. The proportion of low-frequency components is relatively large, concentrated in the range of 0–200 Hz. The frequency of the main shock wave of the first shock event is concentrated in the range 0–50 Hz, and the dominant frequency of the largest amplitude is 24 Hz, of which 0–50 Hz accounts for about 87.2%, and 50–100 Hz accounts for about 12.8%. The frequency of the main shock of the second shock event is concentrated in the range 0–100 Hz, and the main frequency of the largest amplitude is 10 Hz, of which 0~100 Hz accounts for 52.4%, 110–200 Hz accounts for 38.5%, and 210–400 Hz accounts for 9.4%. The main shock frequency of the third event is concentrated in the range of 0–50 Hz; the main frequency of the largest amplitude is 30 Hz, of which 0–50 Hz accounts for about 68.4%, 50–100 Hz accounts for about 20.4%, and greater than 100 Hz accounts for about 12.2%.

The causes of rock burst in these two mines are as follows: coal mining affects the overlying breccia bed; activity such as coal seam deep hole pressure relief blasting and coal seam deep hole water injection failed to effectively relieve the risk of rock burst. The mining layout is unreasonable, the return air is arranged

in the stress concentration coal pillar, and the stress change is unstable when driving through the coal seam. Analyses of the shock waves show that the low-frequency component of the main shock event accounts for a large proportion, and the main frequency is mainly distributed between 5 and 50 Hz.

Study on the stability of the surrounding rock of the roadway

Model establishment and boundary condition setting

The plane model was established using the ANSYS software. The roadway was positioned at the center of the model, the section is rectangular, and the width × height is 5 m×3 m. For the static load calculation, the left and right sides of the model are restrained by horizontal hinges, the bottom is fixed, the upper boundary is free, and the overburden load applied is Q = γH, where γ is the average bulk density of the overburden (γ = 18 kN/m^3), and H is the height of the overburden (m). Assuming that the buried depth H is 600 m, the vertical stress applied to the upper boundary of the model is σy = γH = 10.8 MPa. The model incorporates the characteristics of a homogeneous rock mass. The physical parameters are shown in Tab. 1, and the boundary conditions and grid division of the model are shown in Fig. 5.

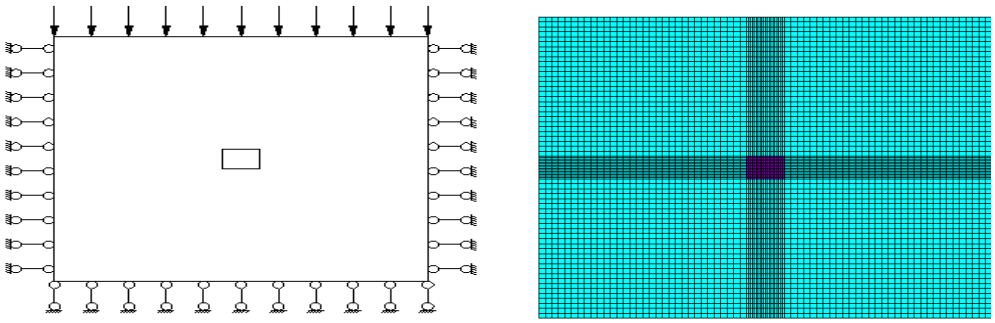

(a) Model boundary conditions (b) Model meshing diagram

Fig. 5. Model diagram

Tab. 1. Physical and mechanical parameters of the rock mass in the numerical calculation model

stratum name	density(kg/m^3)	compressive strength (MPa)	tensile strength (MPa)	cohesion c (MPa)	internal friction angle φ(°)	Elastic model E (GPa)	Poisson's ratio μ
Sandstone	1800	40	2.8	1.2	20	20	0.30

The constitutive model adopted in this simulation is the extended D-P strength criterion, as shown in formula (1):

$$F = Q + \alpha\sigma_m - K \tag{1}$$

Where, $Q = \frac{(\sqrt{3}-\alpha^2)\sin\varphi}{\sqrt{1-3\alpha^2}}$, $K = \frac{c(\sqrt{3}-\alpha^2)\cos\varphi}{\sqrt{1-3\alpha^2}}$

According to plastic theory, the flow rule associated with the extended D-P strength criterion is as follows:

$$d\varepsilon_{ij}^{p} = \lambda \frac{\partial F}{\partial \sigma_{ij}} \tag{2}$$

Where, c—cohesion, MPa; φ— Internal friction angle, °.

The extended D-P strength criterion in the ANSYS software needs three parameters to be set: the constant of the rock material, α; the yield strength, *K,* and the increment of the plastic strain, λ, were generally the most conservative values used in this study. With φ=20° and c=1.2 MPa, it can be calculated that α=0.5, K=2.4 MPa, and $\lambda = 0.5$.

Numerical calculation scheme design and dynamic load waveform input

Scheme design

In this study, the impact location, roadway buried depth, vibration wave frequency, amplitude, and roadway section shape were considered. The values were set as follows: impact position: set the position 10 m away from the roadway roof at 0°, define the angle clockwise, and define the angle between the impact position of the seismic wave and the center of the roadway, θ = 0°, 45°, 90°, and 180°. Roadway buried depth: H = 400 m, 600 m, 800 m, and 1000 m. Vibration wave frequency: f = 20 Hz, 40 Hz, 60 Hz, and 80 Hz. Vibration wave amplitude: a = 0.5 m/s^2, 1.0 m/s^2, 1.5 m/s^2, and 2.0 m/s^2. Roadway section: rectangular, circular, straight wall arch, and horseshoe shape, and the roadway section area is defined as 15 m^2. The simulation adopts a position 10 m away from the center of the roadway. The specific plan is as follows:

(1) We set the seismic wave acceleration amplitude value, impact position, buried depth of the roadway, and the rectangular section shape, that is, when a = 2.0 m/s^2, θ = 180°, H = 600 m, we set different frequencies of f = 20 Hz, 40 Hz, 60 Hz, and 80 Hz.

(2) We set the seismic wave acceleration amplitude value, frequency, buried depth of the roadway, and the rectangular section shape, that is, when a = 2.0 m/s^2, f = 40 Hz, H = 600 m, we changed the impact position to θ = 0°, 45°, 90°, and 180°.

(3) We set the seismic wave acceleration amplitude, frequency, wave incidence angle, and the rectangular section shape, that is, when a = 2.0 m/s^2, f = 40 Hz, θ = 180°, we used a buried depth of H = 400 m, 600 m, 800 m, and 1000 m.

(4) We set the buried depth, frequency, impact position, and the rectangular section shape of the roadway, that is, when H = 1000 m, f = 40 Hz, θ = 180°, we used a vibration wave amplitude of a = 0.5 m/s^2, 1.0 m/s^2,

1.5 m/s^2, and 2.0 m/s^2.

(5) We set the buried depth, frequency, impact position, and seismic wave acceleration amplitude value, that is, when H = 1000 m, f = 40 Hz, θ = 180°, a = 2.0 m/s^2, we changed the shape of the roadway section to be rectangular, circular, a straight wall arch, and horseshoe-shaped.

Selection of damping and numerical calculation of transient dynamics

Rayleigh damping is commonly used to simulate geotechnical dynamics. The expression of Rayleigh damping is as follows:

$$\alpha = 4\pi f_i \frac{\delta}{f_i + f_j} \tag{3}$$

$$\beta = \frac{\delta}{\pi} \Big/ (f_i + f_j) \tag{4}$$

In the formula: α is the mass damping coefficient, β is the stiffness damping coefficient, and δ is the damping ratio. Generally, the value is about 2% to meet the requirements of numerical calculation. To calculate the damping coefficient of the structure, a modal analysis was performed on the model. After completing the modal analysis, a list of the natural frequencies of each order was obtained, and the first natural frequency f_1 and the sixth natural frequency f_6 of the structure were selected. According to the damping, we calculated the mass damping coefficient and the stiffness damping coefficient with a ratio of δ = 2%. The results of the modal analysis of the structure using the ANSYS software are as follows:

SET	TIME/FREQ	LOAD STEP	SUBSTEP	CUMULATIVE
1	19.739	1	1	1
2	22.932	1	2	2
3	30.271	1	3	3
4	31.392	1	4	4
5	39.008	1	5	5
6	45.779	1	6	6

Using f_1 = 19.739 and f_6 = 45.779 in the above equation, we obtain α=0.0758, β=0.000097.

Dynamic load conditions

This model adopts the method of excavating first and then applying the seismic source, which is more in line with the on-site shock situation. The action time of the applied acceleration waveform is 0.05 s, the acceleration amplitude is a = 2.0 m/s^2, and the constitutive model used in the transient dynamics simulation is the extended D-P intensity criterion; the dynamic disturbance can be used in the numerical simulation

calculation of a sine pulse distribution load that is a harmonic in the load waveform, as shown in Fig. 6.

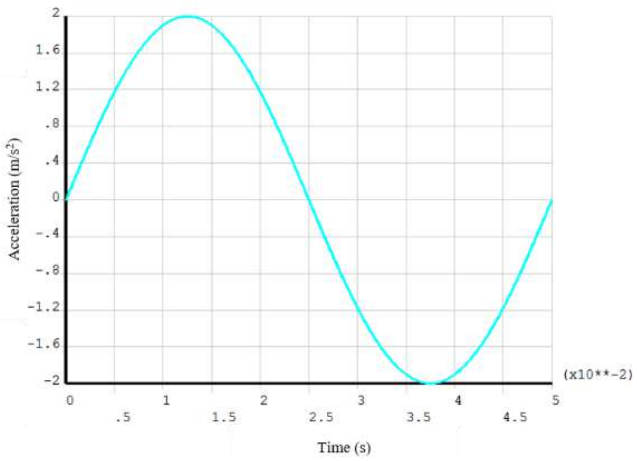

Fig. 6. Sinel waveform

According to energy theory, rock burst is a dynamic phenomenon wherein coal and rock are destroyed rapidly and release a large amount of deformation energy (elastic deformation energy and plastic deformation energy) instantaneously. The occurrence of rock burst depends significantly on the degree of stress concentration and energy accumulation in the surrounding rock, and the level of rock burst mainly depends on the degree of local energy accumulation in the surrounding rock. The higher the degree of energy accumulation in the surrounding rock, the greater the probability of a rock burst. Therefore, the simulation in this study is based on the distribution characteristics of plastic strain energy density to evaluate the tendency for the surrounding rock to impact the roadway in the mines.

Analysis of the simulation results under dynamic load

Change frequency

Fig. 7 shows the distribution of plastic strain energy density at different frequencies.

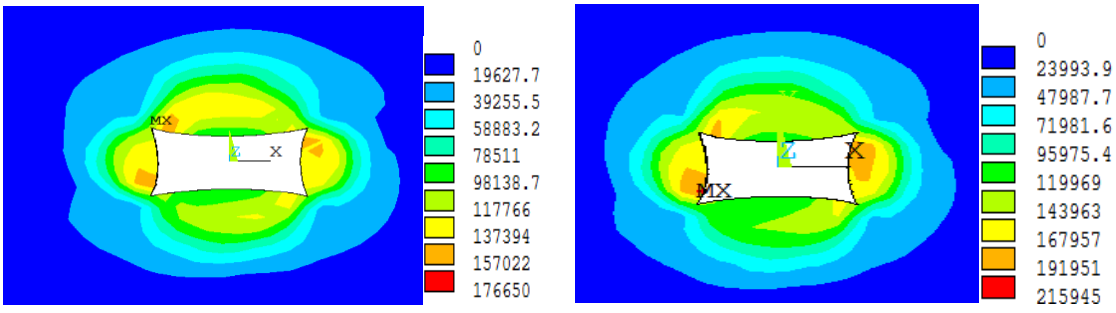

(a) f = 20 Hz (b) f = 40 Hz

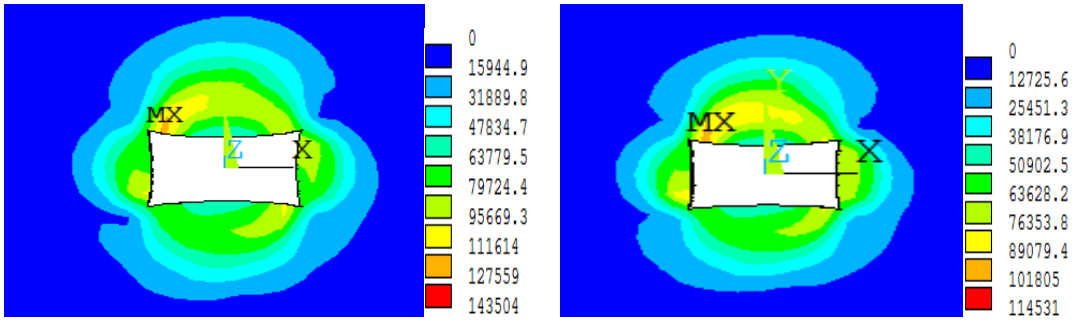

(c) f = 60 Hz (d) f = 80 Hz

Fig. 7. Distribution of plastic strain energy density at different frequencies.

According to the experimental results in Fig. 7, the relationship curve between the maximum plastic strain energy density and frequency was drawn, as shown in Fig. 8.

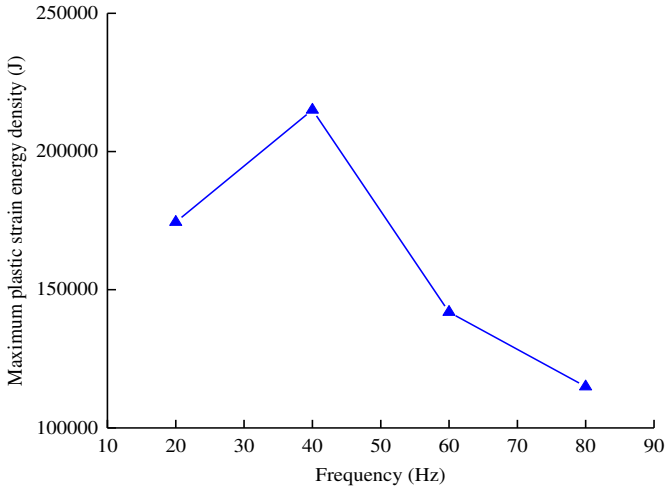

Fig. 8. The relationship between the maximum plastic strain energy density and frequency

It can be seen from Fig. 8 that the distribution of the plastic strain energy density is mainly concentrated around the section of the roadway where the arch angle of the roadway is the largest. When the frequency is 20 Hz, the maximum plastic strain energy density is 1.77×10^6 J; when the frequency is 40 Hz, the maximum plastic strain energy density is 2.16×10^6 J; when the frequency is 60 Hz, the maximum plastic strain energy density is 1.44×10^6 J; when the frequency is 80 Hz, the maximum plastic strain energy density is 1.15×10^6J. Therefore, the order of magnitude of the plastic strain energy density caused by the frequency factor is: 40 Hz > 20 Hz > 60 Hz > 80 Hz; therefore, when a = 2.0 m/s^2, θ = 180°, H = 600 m, and f = 40 Hz, the tendency of the surrounding rock to impact the roadway is higher.

Changing the incident angle of the shock wave

Fig. 9 shows the distribution of the plastic strain energy density under different shock wave incidence angles.

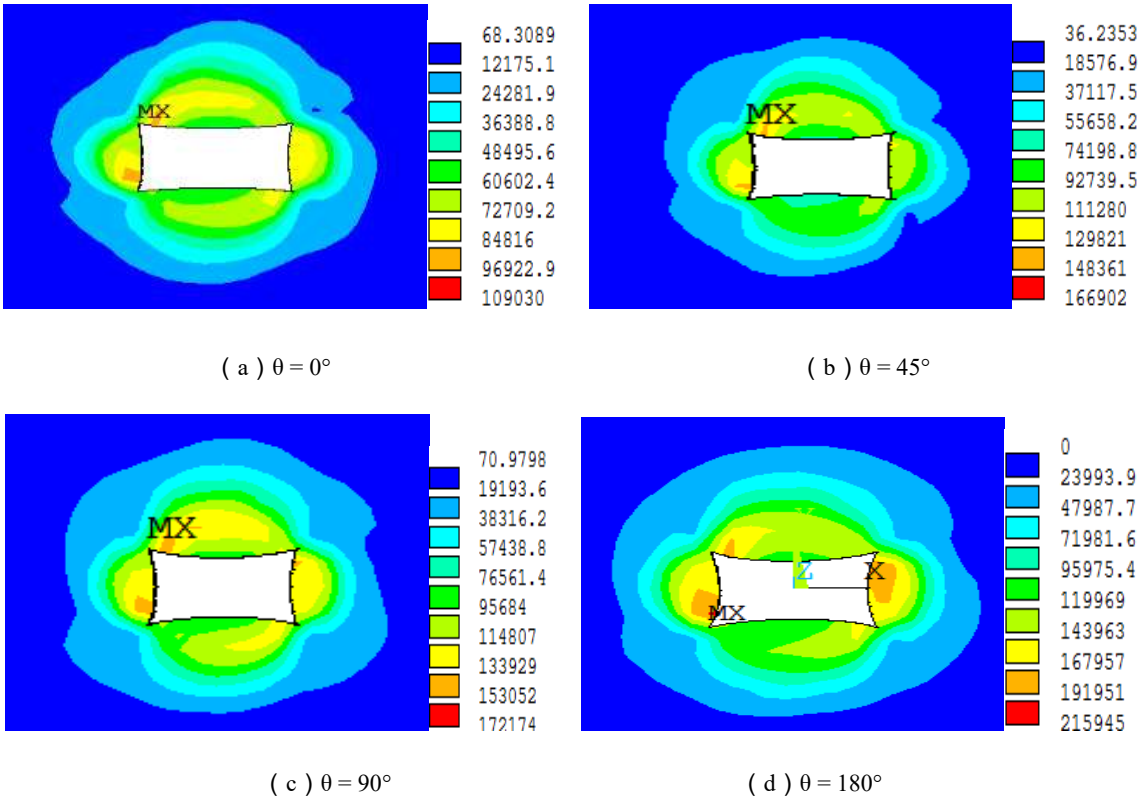

Fig. 9. Distribution of the plastic strain energy density under different shock wave incidence angles.

Based on the experimental results in Fig. 9, the relationship between the maximum plastic strain energy density and the impact position was drawn, as shown in Fig. 10.

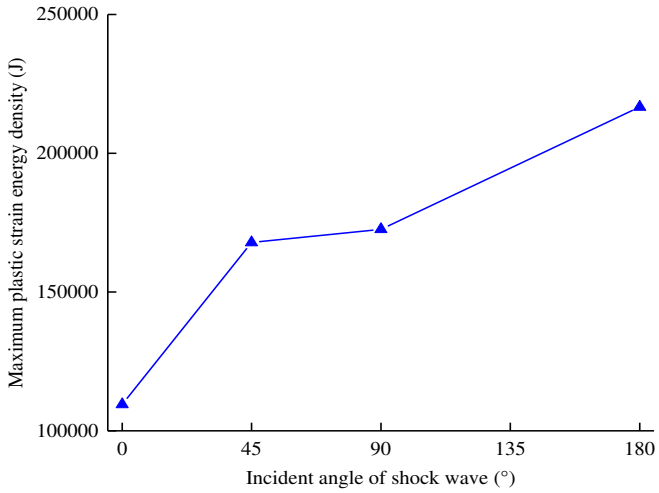

Fig. 10. Relationship curve between the maximum plastic strain energy density and impact position

It can be seen from Fig. 10 that when θ = 0°, the maximum plastic strain energy density is 1.09×10^6 J. When θ = 45°, the maximum plastic strain energy density is 1.67×10^6 J. When θ = 90°, the maximum plastic strain energy density is 1.72×10^6 J. When θ = 180°, the maximum plastic strain energy density is 2.16×10^6 J. Therefore, the order of the magnitude of the plastic strain energy density caused by the impact position is:

180° > 90° > 45° > 0°; therefore, when a = 2.0 m/s^2, f = 40 Hz, H = 600 m, and θ = 180°, the tendency of the surrounding rock to impact the roadway is higher.

Changing the buried depth of the roadway

Figure 11 shows the distribution of the plastic strain energy density at different depths.

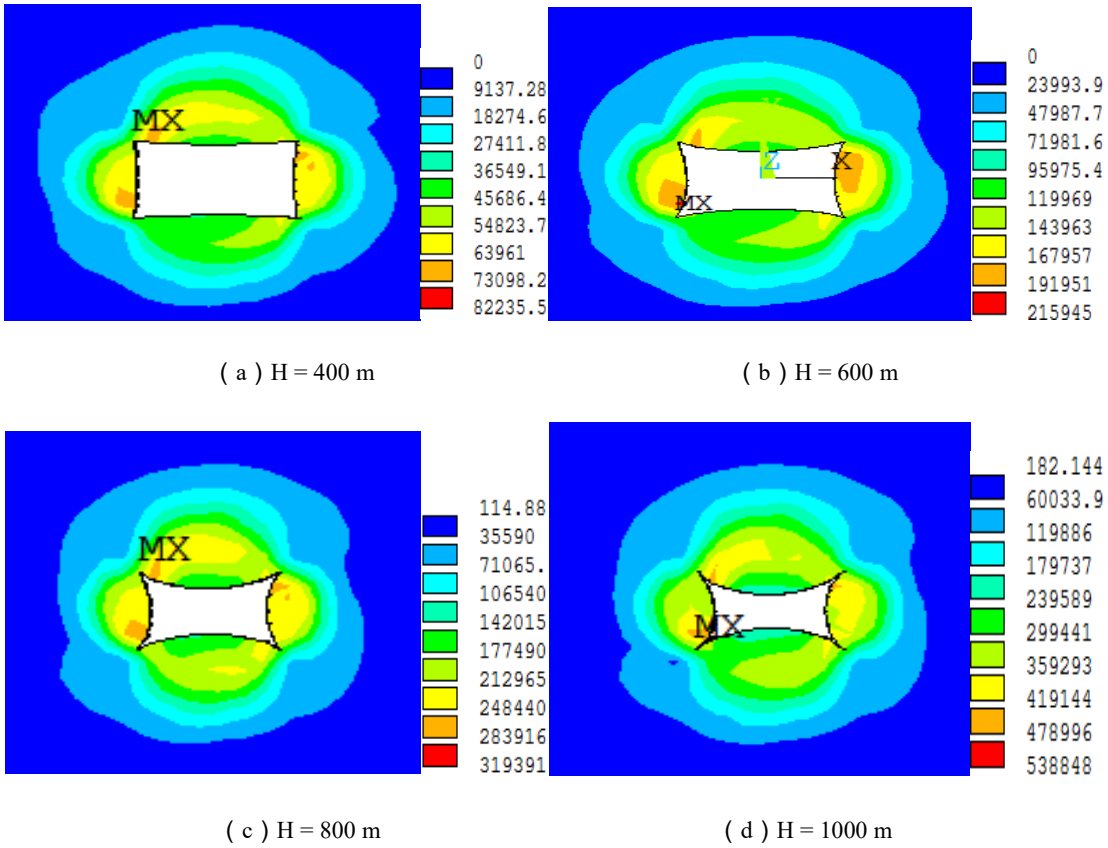

(a) H = 400 m (b) H = 600 m

(c) H = 800 m (d) H = 1000 m

Fig. 11. Distribution of the plastic strain energy density at different depths

Based on the experimental results in Fig. 11, the relationship between the maximum plastic strain energy density and the buried depth was drawn, as shown in Fig. 12.

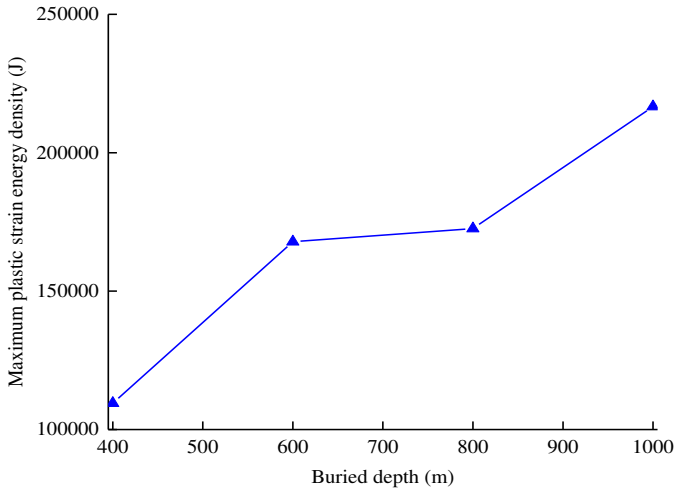

Fig. 12. Relationship curve between the maximum plastic strain energy density and the buried depth of the roadway

It can be seen from Fig. 12 that when the buried depth H = 400 m, the maximum plastic strain energy density is 8.2 × 105 J. When the buried depth H = 600 m, the maximum plastic strain energy density is 2.16 × 10^6 J. When the buried depth H = 800 m, the maximum plastic strain energy density is 3.19 × 10^6 J. When H = 1000 m, the maximum plastic strain energy density is 5.39 × 10^6 J. Therefore, the order of the magnitude of the plastic strain energy density caused by the buried depth of the roadway is: 1000 m ＞ 800 m ＞ 600 m ＞ 400 m; therefore, when a = 2.0 m/s^2, f = 40 Hz, H = 1000 m, and θ = 180°, the tendency of the surrounding rock to impact the roadway is higher.

Changing the shock wave acceleration

Fig. 13 shows the distribution of the plastic strain energy density under different acceleration conditions.

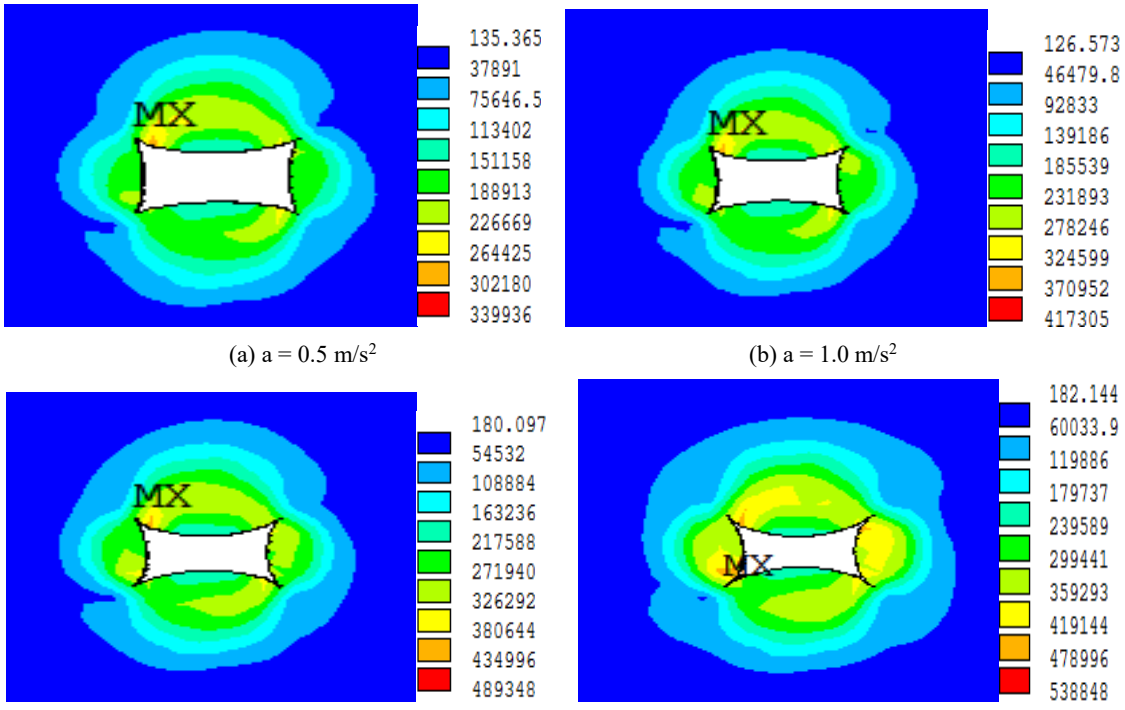

(a) a = 0.5 m/s^2 (b) a = 1.0 m/s^2

(c) a = 1.5 m/s^2 (d) a = 2.0 m/s^2

Fig. 13. The distribution of the plastic strain energy density under different acceleration conditions

Based on the experimental results in Fig. 13, we drew the relationship curve between the maximum plastic strain energy density and acceleration, as shown in Fig. 14.

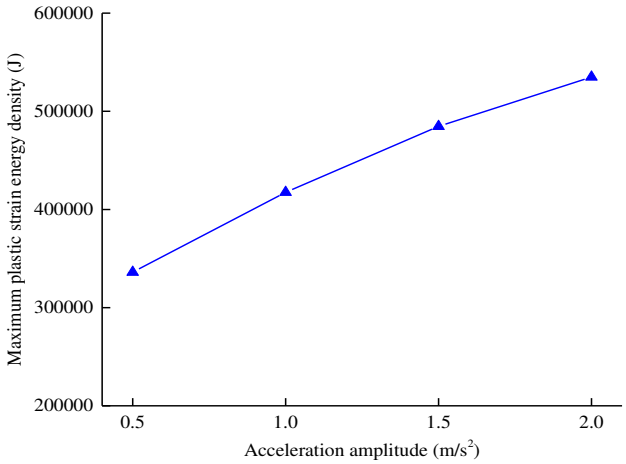

Fig. 14 Relationship curve between the maximum plastic strain energy density and the acceleration amplitude

It can be seen from Fig. 14 that when the acceleration a = 0.5 m/s^2, the maximum plastic strain energy density is 3.40×10^{6}J. When the acceleration a = 1.0 m/s^2, the maximum plastic strain energy density is 4.17 × 10^6 J. When the acceleration a = 1.5 m/s^2, the maximum plastic strain energy density is 4.89×10^{6}J. When the acceleration a = 2.0 m/s^2, the maximum plastic strain energy density is 5.39×10^6 J. Therefore, the order of magnitude of the plastic strain energy density caused by different waveform acceleration amplitudes is: 2.0 m/s^2 ＞ 1.5 m/s^2 ＞ 1.0 m/s^2 ＞ 0.5 m/s^2. Therefore, when a = 2.0 m/s^2, f = 40 Hz, H = 1000 m, and θ = 180°, the tendency of the surrounding rock to impact the roadway is higher.

Changing the cross-section shape of the roadway

Fig. 15 shows the distribution of the plastic strain energy density under different roadway cross-section shapes.

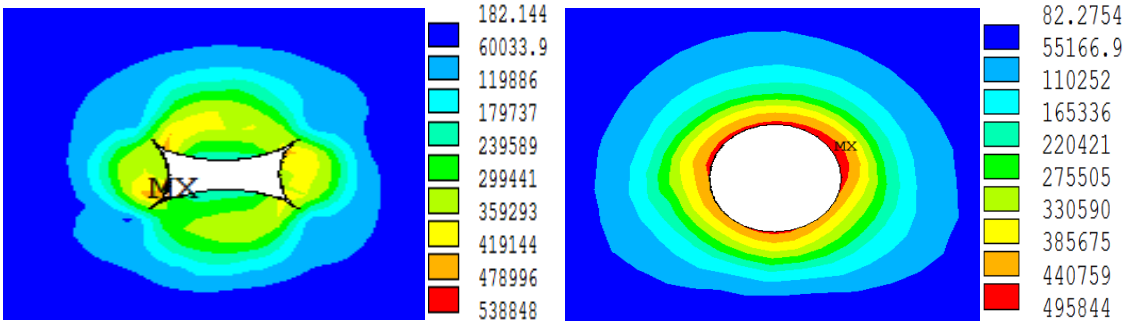

(a) Rectangle (b) Circle

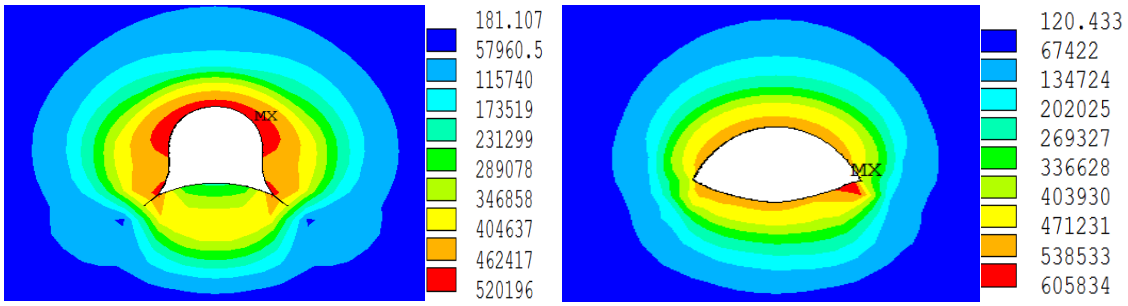

(c) Straight wall arch (d) Horseshoe

Fig. 15. The relationship curve between the maximum plastic strain energy density and the cross-sectional form

It can be seen from Fig.15 that when the section shape is rectangular, the maximum plastic strain energy density of 5.39 × 10^6 J is mainly concentrated at the four arched corners of the roadway. When the section shape is circular, the maximum plastic strain energy density of 4.96 × 10^6 J is mainly concentrated on the roof of the roadway. When the section shape is a straight wall arch, the maximum plastic strain energy density of 5.20 × 10^6 J is mainly concentrated in the roof and arch foot positions of the roadway. When the section shape is horseshoe-shaped, the maximum plastic strain energy density of 6.06 × 10^6 J is mainly concentrated at the arch of the roadway floor.

Therefore, the order of magnitude of the plastic strain energy density caused by different section shapes is: horseshoe section > rectangular section > straight wall arch section > circular section; therefore, when a = 2.0 m/s^2, f = 40 Hz, H = 1000 m, θ = 180°, and the roadway section is horseshoe-shaped, the tendency of the surrounding rock to impact the roadway is higher.

Conclusion

In this study, rock bursts in the Yi coal mine area are analyzed, and the response characteristics of the surrounding rock of the roadway under dynamic load are studied using a numerical simulation method; the following results are obtained:

(1) The main causes of rock bursts are the damage to the overlying gravel strata caused by coal mining and an unreasonable mining layout.

(2) The duration of the shock wave is more than 0.06 s, and the proportion of low-frequency components is large; the main frequency is concentrated in the range of 5–50 Hz.

(3) Taking the distribution characteristics of plastic strain energy density to judge the tendency for rock bursts to occur on the roadway, this study shows that when a (vibration wave amplitude) = 2.0 m/s^2, f (vibration wave frequency) = 40 Hz, H (roadway buried depth) = 1000 m, θ (the angle between the impact

position of the seismic wave and the center of the roadway) = 180°, and the roadway section is horseshoe-shaped, the tendency of the surrounding rock to impact the roadway is higher. Under the same conditions, the impact tendency of the surrounding rock on the roadway is the smallest and second smallest when the roadway is circular and straight-wall arched, respectively.

Acknowledgements

This work was supported by National Natural Science Foundation of China (No. 51974104, 51674101), Henan Science and Technology Research Project (182102210317) and Henan University Basic Research Business Expense Special Funds Subsidy Project (NSFRF180402).

Ethics declarations

The full text or part of the paper has not been submitted or published elsewhere.

Conflicts of interests

The authors declare that they have no competing interests.

References

[1] The State Administration of mine safety issued the analysis report on safety demonstration and special supervision of rock burst mines, China Energy News, 2021.02

[2] Jiang Y. Mechanism and experimental study of coal rock impact instability [M]. Beijing: Science Press, 2009.

[3] Dou L, He X. Theory and technology of rock burst prevention [M]. Xuzhou: China University of mining and Technology Press, 2001.

[4] He M, Jiang Y, Zhao Y. Rock burst control theory based on composite energy conversion[M]. Beijing: Science Press, 2005.

[5] Qian Q. Definition, mechanism, classification and quantitative forecast model for rockburst and pressure bump [J]. Rock and Soil Mechanics, 2014, 35(1): 1-6.

[6] Pan Y, Dai L. Theoretical formula of rock burst in coal mines [J]. JOURNAL OF CHINA COAL SOCIETY, 2021, 46(3): 789-799.

[7] Dou L, Feng L, Cai W, et al. Seismo-acoustic precursor identification and comprehensive warning model for the catastrophic failure process of coal and rock [J]. Journal of Mining & Safety Engineering, 2020, 37(5): 960-968+976.

[8] Yang Y, Wei S. Simulation Study on Mechanical Characteristics of Surrounding Rock of Deep Roadway

under Dynamic Load [J]. Chinese Journal of Underground Space and Engineering. 2020, 16(S2): 664-674.

[9] Jin J, Yang Y, Liao Z, et al. Effect of dynamic load and geo-stress on response characteristics of rock[J]. Chinese Journal of Rock Mechanics and Engineering, 2021.

[10] Xia Y, Feng M, Wang S, et al. Risk assessment method of rock burst based on the combination of theory and field detection [J]. Journal of Mining And Strata Control Engineering, 2021.

[11] Song J, Lu C, Li Z, et al. Characteristics of stress distribution and the law of microseismic activity in rock parting occurrence area [J]. Journal of Mining and Strata Control Engineering, 2021, 3(4): 043518.

[12] Jiao J. Analysis on influencing factors of stability of anchorage bearing structure of roadway under dynamic load [J]. Journal of Henan Polytechnic University (Natural Science), 2021, 40(4): 19-27.

[13] Wang P, Zhou H, Wan G, et al. Stress characteristics of different mining directions adjacented fault under hard thick roof [J]. Journal of Mining and Strata Control Engineering, 2021, 3(4): 043529.

[14] He J, Wu Y, Fu Y. Mechanics response law of surface protecting components for rock bolting under impact load [J]. Journal of Mining & Safety Engineering. 2021, 38(3): 556-564.

[15] Wu Z, Pan P, Pan J, et al. Analysis on mechanism of rock burst and law of mine earthquake activity in graben structural area [J]. Rock and Soil Mechanics, 2021-05-07.

[16] Cui F, Zhang T, Lai X, et al. Research on mining disturbance characteristics and productivity of rock burst mines under different mining intensities[J]. Journal of China Coal Society. 2021-04-23.